Architecture
Image Studies

Vol.6, Issue 4, pp.312-327, 2025
DOI: https://doi.org/10.62754/ais.v6i4.603

https://journals.ap2.pt/index.php/ais/index

Hybrid Deep Learning Model with Optimization Algorithm for Precise Skin Disease Prediction and Classification

Dhanesh Kumar[1], Dr G Bhuvaneswari[2], Dr G Manikandan[3], Shameem Ansar A[4], Dr. P Vasanth Sena[5], P. Deepa[6]

Abstract

In recent years, developing a cost effective and high efficiency screening mechanism is critical. To resolve these issues, an innovative methodology was presented in this article for identifying skin diseases. Each collected image was initially preprocessed and cropped to a size of pixels. With six square patches, these images are separated into pixels. Subsequently, image augmentation steps including flipping, rotation and image improvement are employed for minimizing the parameter requirements in further processes. The kernel weighted fuzzy local information c-means clustering (K-FCM) methodology was deployed for locating and fragmenting the cancer-affected parts. Consequently, both color and texture attributes are captured. Further, the Deep Long and Short Term Memory (DLTM) based Tunicate Swarm algorithm (TSA) was designed for identifying and categorizing skin diseases as normal or abnormal. This study was modeled in MATLAB and used the experimental image database acquired from Herlev University Hospital in Denmark for validation. As per findings of the comparison analysis, the suggested DLSTM-TSA outperforms the competition in terms ofF-score, sensitivity, accuracy andprecision.

Keywords: *Skin Disease, Tunicate Swarm Algorithm, Deep LSTM, Herlev University Hospital And Performance Metrics.*

Introduction

Skin is the mainappendage of the human body, consisting of subcutaneous, dermis, and epidermal tissues, as well as muscles, nerves, lymphatic veins, and blood vessels, which may protect the body and sense external temperature [1-4]. The skin provides a shield to the whole body, protecting the organs and tissues from various extrinsic invasions like the immune system, infectious viruses, chemical damage, and artificial skin damage. In addition, the skin exhibits barrier operation by preventing the loss of water and lipids within dermis and epidermis.

Since this is the body's biggest organ, the effects of inflammatory, bacterial, and viral diseases travel throughout the body, causing a wide range of health problems [5]. Vitiligo, wrinkles, atopic dermatitis, psoriasis, wounds, photo ageing, melanoma, morphea, alopecia, acne, and other skin problems are among them. Many of these diseases can be healed if they are caught early enough before they spread [36]. Dermoscopy is a technique that uses polarization to reduce surface reflection and is used by professionals to study skin changes with the use of a strong light.

Despite its barrier and defensive characteristics, it is consistently influenced by various exterior and genetic variables. At present, the skin is affected by three skin diseases such as viral skin infection, allergic skin disorder, and fungal skin disease [6-8]. Although many of the skill infections are recoverable, they create distress to the patients. These diseases are identified by the clinical

[1] Assistant Professor, Department of Computer Science and Engineering, Koneru Lakshmaiah Education Foundation, Vaddeswaram-522302, Guntur, Andhra Pradesh, India, Email: dhaneshkresearch@gmail.com (corresponding author).
[2] Professor / CSE, Department of Computer Science and Engineering, Saveetha Engineering College, Saveetha Nagar, Sriperumbadur Taluk, Chennai, Tamil Nadu 602105, India.
[3] Professor, Department of Artificial intelligence and Data Science, RMK ENGINEERING COLLEGE RSM Nagar, Kavaraipettai, Gummidipoondi Taluk, Tiruvallur District, Tamil Nadu, India
[4] Dept. of Computer Science and Engineering, TKM College of Engineering Kollam,India
[5] Assitant Professor, Department of CSE, GNITS,Hyderabad,Telanagana,India
[6] Assistant professor, Department of CSE, SNS College of technology, Coimbatore, India

professionals and its accuracy depends on their experience. This way of disease prediction is prone to error, which results in treatment delays.

It's possible that the skin lesions are either primary or secondary [9]. Bulla, cyst, pustule, vesicle, tumour, nodule, discolouration, spots, pimples and plaque becomes main skin lesions, when atrophy, maceration,umbilication,phyma,ulcer,fissure,induration, excoriation, and erosion are secondary skin lesions. Distribution and configuration are two words that are connected to skin lesions [37]. The pattern denotes the lesionsgrouping, while the sharing denotes the location of lesions. Based on the basic three types of skin infections are mostly studied in the literature, more skin connected image segmentation and classification are covered in this work. Likewise, supervised methods grouping such as SVM are widely used, but they have a number of essential parameters that must be identified and set correctly to obtain better results and more precise classifications. To tackles the challenges in the existing study, we proposed DLTM based TSA is introduced for predicting skin diseases.

The remaining portions of the article are arranged as: Section 2 describes the related studies followed by the proposed methodology and is delineated in Section 3. The implementation outcomes are discussed in Section 4. Finally, in section 5, the paper is completed.

Related Works

Bhadula et al. [10] designed machine learning (ML) methods to categorize skin diseases. To predict the exact kind of skin disease, five different ML algorithms were chosen and used for a data collection of skin infections. We've worked with CNN, kernel SVM, logistic regression, naive bayes (NB), and Random forest, among a few ML approaches. A comparable investigation based on training accuracy and confusion matrix parameters has been carried out and graphed. CNN has been discovered to have the highest training precision for the correct prediction of skin disorders of all the candidates and this method is not applicable for real time data.

Chakraborty et al. [11] developed an integrated neural network incorporated with a bag of attributes for image based skin disease diagnosis. The bag-of-features altered information can be used to train metaheuristics-asserted hybrid ANN to classify images of skin to diagnose the disorders under investigation. In this work, Non-dominated Sorting Genetic Approach-II was employed for training the ANN (NN-NSGA-II). The implementation results are determined in terms of recall, f-measure, precision and accuracy. Also, a comparative assessment was conducted with two meta-heuristic algorithm assisted classifier models such as ANN assisted with PSO and ANN-incorporated with Cuckoo search, and it manifested that the developed NN-NSGA-II has earned improved results.

Machine learning and image processing (ML-IP) was presented by ALEnezi et al. [12] for the diagnosis of skin disease. This approach considers the digital photograph of the skin image and uses image processing to detect disease types. This framework is easy and uncomplicated with less requirement of expensive components rather than a system and a camera. The retrained convolutional neural system was deployed for capturing the distinct attributes that are further categorized by utilizing multiclass SVM. Moreover, this framework has the effectiveness of identifying the disease type and its severity. The experimental findings illustrated that it obtained 100% accuracy in disease categorization.

Balaji et al. [13] introduced the use of a dynamic graph cut (GC) method with a NB (GC-NB) model for skin disease identification and categorization. The researchers wanted to use a new dynamic GC algorithm for skin lesion fragmentation, and used an NB classifier to categorise disease type. This methodology was tested using the ISIC 2017 database and found that it achieved better outcomes than conventional approaches like FCN and SegNet. The designed algorithm obtained 92.9% accuracy in identifying benign instances and 91.2% accuracy in detecting melanoma.

Khamparia et al. [14] designed a deep learning (DL) algorithm to perform skin cancer classification. Fully automated features have been extracted from images utilising distinct pretrained configurations such as SqueezeNet, ResNet50, Inception V3 and VGG19, and fed into a fully connected layer of CNN. Completely integrate with an IoHT architecture and capable of assisting specialist doctors in the management and therapy of skin cancer from a distance. The suggested system beat existing pretrained designs considering the metrics like accuracy, recall, and precision in classifying skin cancer from skin lesion images, according to performance metric evaluation.

Proposed Model:

The general architecture of the developed framework is displayed in Figure 1. The developed methodology involves four stages namely: preprocessing, segmentation, feature engineering and skin

categorization. Finally, the model's precision, specificity, recall, AUC, and F-score are evaluated. The subsections below provide a more detailed explanation of each stage.

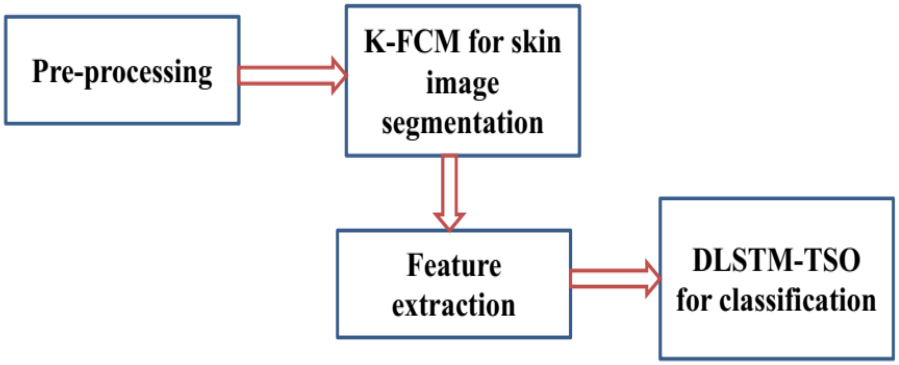

Figure 1: Proposed Architecture

Pre-processing:

Various normal and abnormal images in JPG format were acquired from three different classes. All JPG images have a primary matrix size of $1238*`1336$pixels. For each image, we first run a pre-processing step [15]. The images are first cropped into $518*`518$ pixels, and then each one is divided into pixels using six square patches. Resize every original image into $224*`224$ after that. The originalimages of 2112 are finally received.

Skin Image Segmentation Based on K-FCM:

While thinking that neighbourhood information affects current pixels, the FLICM method never has a regularisation parameter for fuzzy local information factor [16]. To improve the FLICM robustness to outliers and noises, Memonet al. [17] suggested the KFCM model by developing the kernel parameter and trade off weighted fuzzy factor. The KFCM model is utilized to segment cervical cancer images in this investigation.

$$J_{KFCM}(A,B)=\sum_{l=1}^{N}\sum_{k=1}^{D}b_{lk}^{n}\left(\left\|\phi(z_l)-\phi(c_k)\right\|^2+G_{lk}\right) \quad (1)$$

The total sample and cluster counts are defined as N and D respectively. The membership function z_l of the l^{th}cluster is b_{lk} in which a nonlinear map is denoted by ϕ. The objective of image segmentations is described by Equation (2).

$$J_{KFCM}(A,B)=\sum_{l=1}^{N}\sum_{k=1}^{D}b_{lk}^{n}\left[(1-K(y_l,a_k))+G_{lk}\right] \quad (2)$$

From this, fuzzy local feature is G_{lk} in which it current pixel's memebership data, local geographical and grey information.

$$G_{lk}=\sum_{i\in N_{l,l\neq k}}\frac{1}{I_{l,k}}W_{lk}(1-a_{lk})^{n}(1-K(z_k,b_i)) \quad (3)$$

Around the degree of membership pixel z_l, the closer pixel falling to the window is depicted as z_z. A Euclidian distance ofspatial among a pixels z_l and z_k is indicated by the symbol $I_{l,k}$. The factor

of local resemblance becomes W_{lk} . The centre of cluster a_i and a degree of membership a_{il} are expressed as follows.

$$a_{il} = \frac{\left((1-K(z_l,b_k)+G_{il}\right)^{-1/n-1}}{\sum_{k=1}^{d}\left((1-K(z_l,b_k)+G_{il}\right)^{-1/n-1}} \quad (4)$$

$$a_i = \frac{\sum_{j=1}^{M} b_{i,l}^{n} K(z_l,a_i) z_l}{\sum_{j=1}^{M} b_{i,l}^{n} K(z_l,a_i)} \quad (5)$$

In FLICM, the square Euclidian distance is substituted by a Gaussian kernel induced distance measure, which is referred to as KFCM [18]. Thus, the KFCM segments and locates the cancer affected part of the image.

Feature Extraction:

The aim of this process is to take out useful elements from the picture illness region that can aid in disease identification and evaluation [19].

Color Features: The average value for colour in various colour channels is one of the most popular colour attributes. Luminance, grey, Hue and Value (from HSV color-space), Red, Green Blue (RGB), and Chrominance were the colour channels utilised to capture colour differences (from YCbCr colour space). Take out ten features for colour features portrayal in the illnesses region in this article.

Texture Features: Gray Level Co-occurrence Matrix (GLCM) is a grey scale picture matrix. Texture analysis is dependent on most prevalent methods for selecting texture attributes. The image texture is characterised by counting the number of times a pixel with a specified brightness intensity of a skin picture appears in a given spatial direction [20]. The homogeneity, correlation, energy, and contrast properties of the GLCM matrix are employed to define the area.

Skin Disease Detection and Classification:

The DLSTM-TSA are used for skin disease detection and classifications.

Deep Long and Short Term Memory (LSTM):

The prediction representation was urbanized using a conventional ANN that provides a direct mapping amongthe output prediction data and the input historical information [21]. The lack of time correlation in data series captures the link between time and data. The hidden neurons are explained by the equation below.

$$X_f^t = \sum_{j=1}^{I} W_f y_j^t + \sum_{f`=1}^{h} W_{f^{\sim}} Y_{f^{``}}^{t-1} \quad (6)$$

With the input RNN of sequence length *y*, the hidden neurons (*h*), output neurons (*O*), and input neurons (*I*) are shown. The*j*th input value is y_j^t at the *t*-time of *y*. The activation and hidden neurons' network inputs are X_j^t and Y_j^t . The value of the weight parameter is W_f and the backward pass computation technique is described by the following formula.

$$\delta_f^t = \sum_{k=1}^{O} \lambda_k^t W_{jf} + \sum_{f`=1}^{h} W_f \lambda_k^{t+1} \quad (7)$$

$$\delta_f^t = \frac{\partial \psi}{\partial X_i^t} \tag{8}$$

$$\frac{\partial \psi}{\partial X_{ij}} = \sum_{t=1}^{T} \frac{\partial \psi}{\partial X_i^t} \times \frac{\partial X_i^t}{\partial W_{ij}} = \sum_{t=1}^{T} \lambda_i^t Y_j^t \tag{9}$$

The most important benefit of using RNN is its effectiveness to use contextual data, while outlining input and output sequences. The RNN's sensitivity to input is decreased during the early training stages [22]. The performance of a traditional RNN model is increased by using LSTM. The back-propagation through time (BPTT) technique is used to update the neuron weight, with forward and backward rounds training the LSTM-based neurons.

$$X_g^t = \sum_{t=1}^{I} W_{jg} y_j^t + \sum_{H=1}^{h} W_{Gf} B_g^{t-1} + \sum_{d=1}^{D} W_{Df} S_D^{t-1} \tag{10}$$

$$Y_g^t = f\left(X_g^t\right) \tag{11}$$

Forget gates have the following input and output values:

$$X_g^t = \sum_{t=1}^{I} W_{j\rho} y_g^t + \sum_{H=1}^{h} W_{f\rho} Y_f^{t-1} + \sum_{D=1}^{d} W_{D\rho} S_D^{t-1} \tag{12}$$

$$Y_\rho^t = f\left(X_\rho^t\right) \tag{13}$$

The input, state, and output memory cells are defined by the equations below.

$$X_D^t = \sum_{j=1}^{I} W_{jD} y_j^t + \sum_{f=1}^{h} W_{gD} Y_f^{t-1} \tag{14}$$

$$S_D^t = X_f^t H\left(X_D^t\right) + Y_\rho^t S_D^{t-1} \tag{15}$$

$$Y_D^t = Y_W^t F\left(S_D^t\right) \tag{16}$$

For output gates, the output andinput values are as follows:

$$X_W^t = \sum_{j=1}^{I} W_{jW} y_j^t + \sum_{f=1}^{h} W_{gW} Y_f^{t-1} + \sum_{D=1}^{d} W_{DW} S_D^t \tag{17}$$

$$Y_D^t = f\left(X_W^t\right) \tag{18}$$

In the backward pass, upgrade the weight coefficients of LSTM neurons. The connection weights W_{ij} are from *j* to *i* nodes. The memory cell, forget gate, and input gate are W_{DW}, $W_{D\rho}$ and W_{Dg}. *f* is the gate activation function for each memory cell, and *t* is the memory cell state. The off activation functions for input and output memory cells becomes f and the total input value in the hidden unit is described as *H*. Furthermore, the construction of the LSTM-RNN model is depicted in Figure 2.

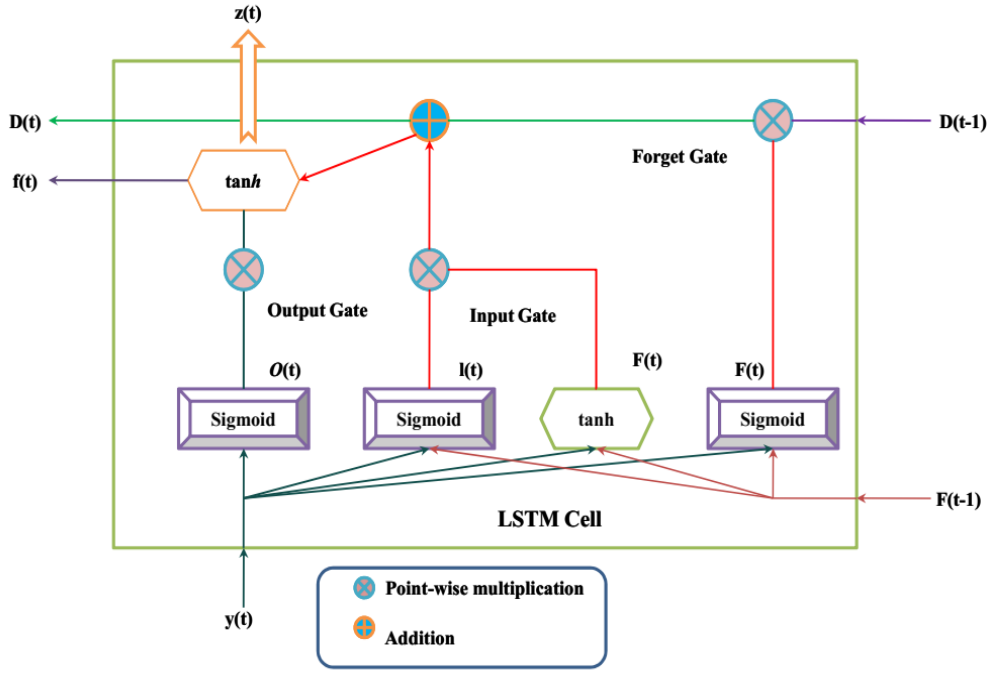

Figure 2: LSTM-RNN Model Construction

TSA:

The tunicate is utilized to find out where seafood is located. Furthermore, tunicate features (Swarm intelligence combined with jet propulsion) identify the best food source [23]. In addition, the jet propulsion must meet three criteria: I proximity to the search agent, ii) ignorance of agent divergence, and iii) progress toward the search agent. The best ideal solution will improve the properties of Swarm. In the next section, we'll look at the numerical expression.

(i) Search Agents' Ignorance of Divergence:

By estimating a new position for the search agent, the divergence among the search agents can be denied.

$$\vec{E} = \frac{\vec{h}}{\vec{n}} \quad (19)$$

$$\vec{h} = x_2 + x_3 - \vec{G} \quad (20)$$

$$\vec{G} = 2.x_1 \quad (21)$$

$\vec{G}$ represents the water flow advection and $\vec{h}$ denotes the gravity force. 'x_1, x_2, and x_3' are the arbitrary variables and lies among 0 to 1 [24]. Moreover, the social force between the search agent is defined by $\vec{n}$.

$$\vec{n} = [r_{\min} + x_1.r_{\max} - r_{\min}] \quad (22)$$

Equation (17) establishes the initial and subordinate speeds are $r_{\min}$ and $r_{\max}$, as well as how they are used to generate social interaction. Let's have a look at the values of $r_{\min}$ and $r_{\max}$ is 1 and 4.

(ii) The path to the best behavior:

After ignoring the neighbor's divergence, the search agents intend to move to the nearby best side.

$$\overrightarrow{IC} = \left| \overrightarrow{fs} - r_{andom} \cdot \overrightarrow{r_p(x)} \right| \quad (23)$$

The distance between the search agent and the food supply is represented here $\overrightarrow{IC}$. For the moment, *x* reflects the tunicate's current execution and determines the food source's location is $\overrightarrow{fs}$. The tunicate position $[Random \in 0,1]$ is denoted by an arbitrary constant $\overrightarrow{r_p(x)}$.

(iii) Rate of convergence:

The rate of convergence amongst search agents is referred to as the convergence rate. The can's upgraded position $\overrightarrow{r_p(x)}$ is indicated by the symbol $\overrightarrow{fs}$.

$$\overrightarrow{r_p(x)} = \begin{cases} \overrightarrow{fs} + \vec{V} \cdot \overrightarrow{IC} & if \quad Random \geq 0.5 \\ \overrightarrow{fs} - \vec{V} \cdot \overrightarrow{IC} & if \quad Random < 0.5 \end{cases} \quad (24)$$

(iv) The swarm's characteristics:

The placement of search agents is improved when the convergence rate is completed to duplicate the tunicate's swarm features.

$$\overrightarrow{r_p(x+1)} = \frac{\overrightarrow{r_p(x)} + \overrightarrow{r_p(x+1)}}{2 + b_1} \quad (25)$$

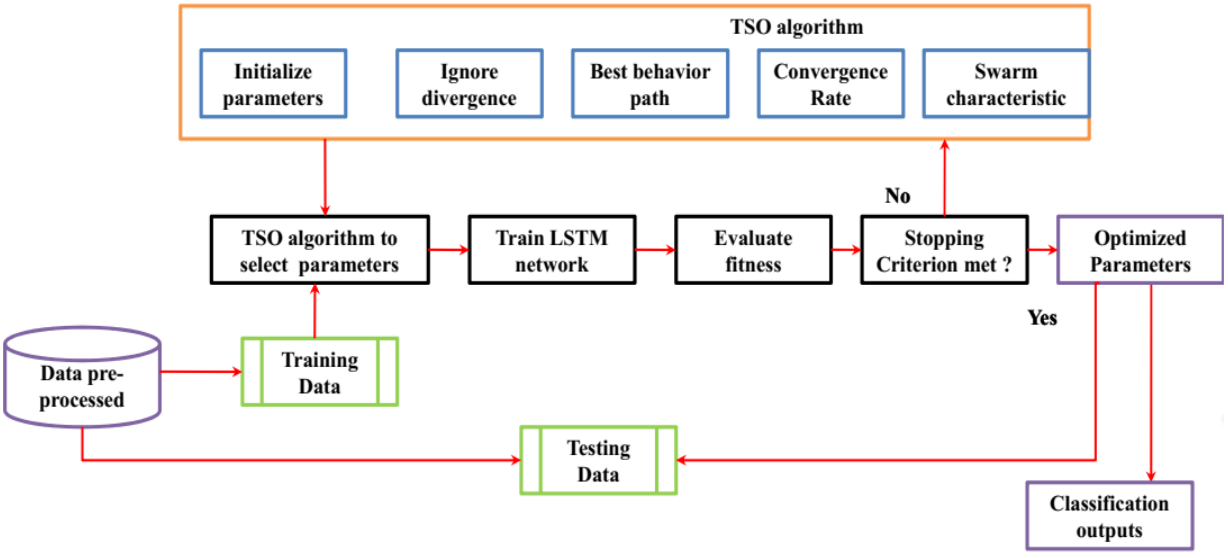

Figure 3: DLSTM Based TSA Algorithm for Skin Disease Classification

LSTM with TSA for Skin Disease Detection:

The DLSTM has several benefits including its capacity to reframe weight coefficients, efficiency to prevent vanishing gradient issue, capacity to fine-tune parameters and more [25-28]. Although, the

DLSTM may contains some drawbacks like overfitting, computational complexity and so on. The Tunicate Swarm Algorithm (TSA) is used for parameter optimization in DLSTM for skin disease detection to address these concerns. This algorithm has enhanced searching efficiency, which results in reduced time consumption and improved search results among other algorithms like ant colony optimization, ant bee colony algorithm, cuckoo search algorithm, chimp optimization algorithm and etc

DLSTM based TSA is used to select the amount of LSTM units and customizable time window during skin disease categorization. A well-chosen time window plays a critical part in a promising performance. When the window is too large, the model overfits the training data. When the window is too small, the model removes the important data. The block diagram of the DLSTM based TSA for skin disease classification is shown in Figure 3. In every hidden layer, the TSA examines the best number of hidden neurons, and two hidden layers follow the proper network designing parameter for DLSTM. The hyperbolic tangent function is used as an activation function in DLSTM's input and hidden layers.

Table 1: parameter settings for the DLSTM-TSA

Parameters	Value
Tunicate's population size	100
Maximum iteration	300
Learning rate	0.001
Modality	0.01
Total fully connected layer units	30
Dropout	0.5
hidden state dimension	50
Batch size	50
Epoch count	10
Power exponent	Linearly reduces from 0.1 to 0.3

The activation function of the output node is designed by the linear operation [29]. The TSA is used to optimise the architectural parameters and the appropriate size of time windows in LSTM. Apply multiple numbers of LSTM units in each hidden layer and different time windows widths to validate the TSA fitness, which is based on the DLSTM, produces better categorization outputs like normal and abnormal cases of kin image.

Result and Discussion

The MATLAB software performs experimental research for skin disease categorization. The developed framework's proficiency is assessed using a variety of tests and state-of-the-art technologies [30-32]. Table 1 shows the parameter settings for the DLSTM-TSA for skin disease analysis.

Dataset Details:

As trial images, we looked at skin diseases from around the world. Dermnet provided us with the photos. We took into account skin infection images with natural parts. It is noted that the model's precision changes in accordance with disease type. We've also gathered images from the internet. More than 500 images have been downloaded for ulcers, stasis dermatitis, lichen simplex chronicus, eczema subcute, eczema nummular, and eczema [33] and [34], which are five distinct illnesses.

Performance Criterions

The performance of the DLSTM-TSA for skin disease identification is validated using assessment metrics such as accuracy, specificity, f-measure, precision, Matthews Correlation Coefficient (MCC), and sensitivity [35].

Accuracy determines the model's efficiency in categorizing the skin diseases, and it is denoted as (A). It is measured using equation (26).

$$A = \frac{Tn + Tp}{Tn + Tp + Fn + Fp} \tag{26}$$

Specificity defines the actual negative proportion that is precisely categorized as negative as follows:

$$Specificity = \frac{Tn}{Fp + Tn} \quad (27)$$

Sensitivity quantifies the actual positive proportion precisely classified as positive, as expressed in equation (28).

$$Sensitivity = \frac{Tp}{Fn + Tp} \quad (28)$$

Precision (P) is defined as the proportion of abnormal predicted classes that is really correct.

$$P = \frac{Tp}{Fp + Tp} \quad (29)$$

The F-measure, which balances precision (P) and recall (R), is the harmonic mean, which evaluates the test accuracy. The recall and F-score formula is calculated using equation (30) and (31).

$$R = \frac{Tp}{Fn + Tp} \quad (30)$$

$$F - score = 2\left(\frac{R \times P}{P + R}\right) \quad (31)$$

It reveals overoptimistic inflated outcomes in the situation of imbalanced datasets. The accuracy and Matthews Correlation Coefficient (MCC) are the most relevant measures for evaluating datasets models. The categorization performance is evaluated using three confusion matrix values. MCC's interval range is -1 to 1. MCC's formula is expressed in equation (32)

$$MCC = \frac{(Tn + Tp) - (Fn \times Fp)}{\sqrt{(Tn + Fn)(Tn + Fp)(Tp + Fn)(Tp + Fp)}} \quad (32)$$

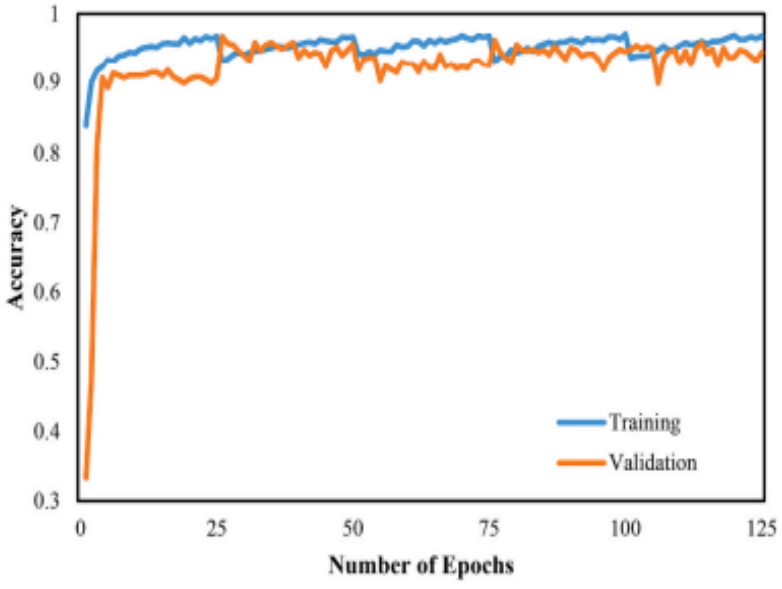

Figure 4: Performance Analysis of Accuracy

Performance Assessment:

Figures 4 and 5 depict the skin disease classification performance analysis with respect to accuracy and loss. Figure 4 depicts the loss assessment across epochs count. The validation and

training accuracies at epochs are 97.0 percent and 98.3 percent, respectively, from Fig 4. Both the training and validation sets had accuracy of over 96 percent. We have obtained 0.07 percent and 0.05 percent validation and training losses, as shown in Fig 5.

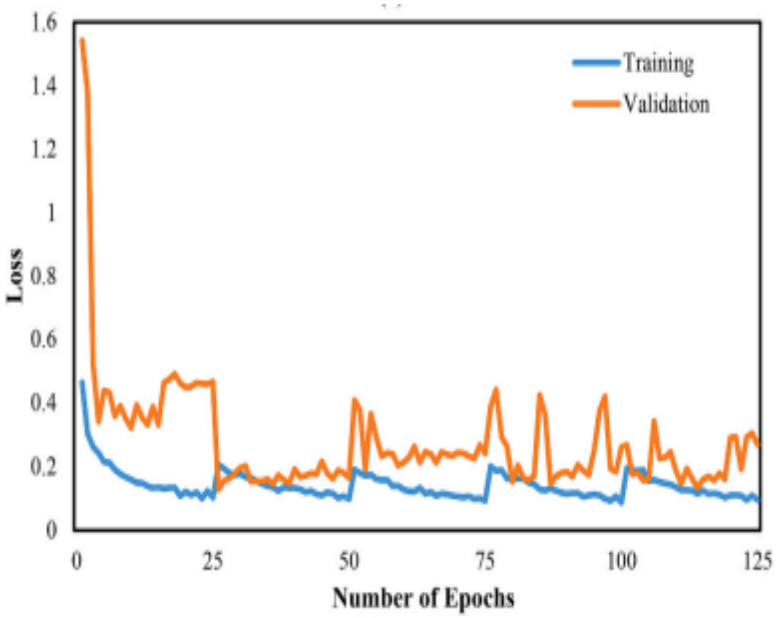

Figure 5: Performance Analysis of Loss

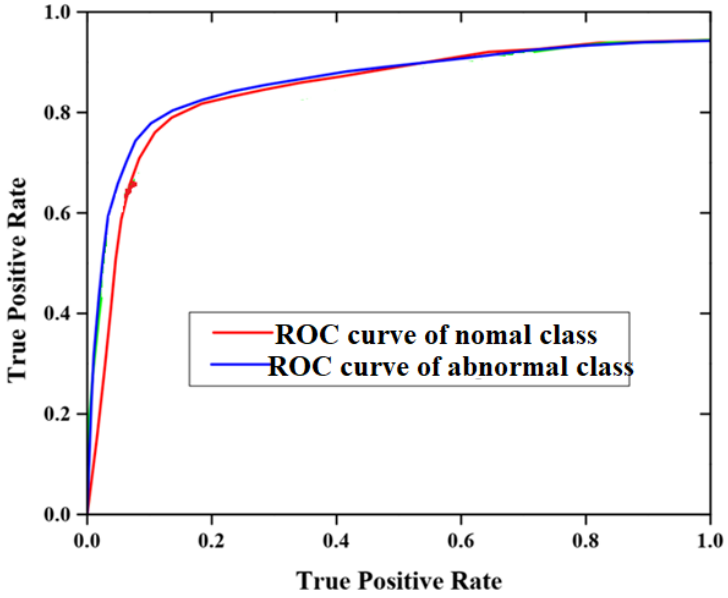

Figure 6: ROC Curve Performance Analysis Based on Normal and Abnormal Classes

Figure 6 shows the performance of each class based on ROC data. The curve between false positive and true positive rates is displayed. The total number of true positive predictions is divided by the sum of the false positive and true positive rates. The rate of a true positive is referred to as recall or sensitivity. The performance of the binary classification model is described in the display of the ROC curve based on the positive class. The balance of predictions might change the classification threshold depending on the trade-off between false positive and true positive rates. The normal and a ROC curves vary in accuracy, reaching 0.88 percent, 0.92 percent, and 0.93 percent, respectively.

Table 2 describes the suggested DLSTM-based TSA for the classification ofskin disease results depending on each class, such as normal and abnormal. We acquired 91 percent precision, 92 percent recall, 91 percent F-measure, and 90 percent accuracy for regular classes. Furthermore, for the

abnormal class, accuracy of 95%, precision of 94 percent, recall of 92 percent, and F-measure of 94 percent are achieved.

Table 2: The Proposed LSTM-RNN Based TSA For Classification of Skin Disease Results Based on Each Class

Classes		Normal	Abnormal
Performance measures	Accuracy	92 %	95%
	F-measure	91 %	94%
	Recall	92 %	92%
	Precision	91 %	94%

We use K-FCM to evaluate improved segmentation outcomes based on structural similarity index measure (SSIM) and DICE parameters. The local correlation (s) between the test images (o) and the reference image pixels used by SSIM is modulated by distortions.

$$SSIM(I_o, I_s) = \frac{(2\delta_o\delta_s + V_1) + (2\sigma_{os} + V_2)}{(\delta_o^2 + \delta_s^2 + V_1)(\delta_o^2 + \delta_s^2 + V_2)} \quad (33)$$

As a result, the average and variances are δ and δ^2 respectively. Where the stabilising factor is V and the covariance of *s* and *o* is σ_{0S}. The DICE measure is used to determine the similarity of two photographs based on the number of shared pixels. DICE is used to quantify the spatial overlap between automatic segmentation and ground truth. Figure 7 shows the proposed segmentation result for each class using the SSIM and DICE measures. When employing K-FCM algorithms, a higher DICE and SSIM value suggests better segmentation outcomes.

$$D = \frac{2|Z \cap Q|}{|Z \cap Q| + |Z \cup Q|} \quad (34)$$

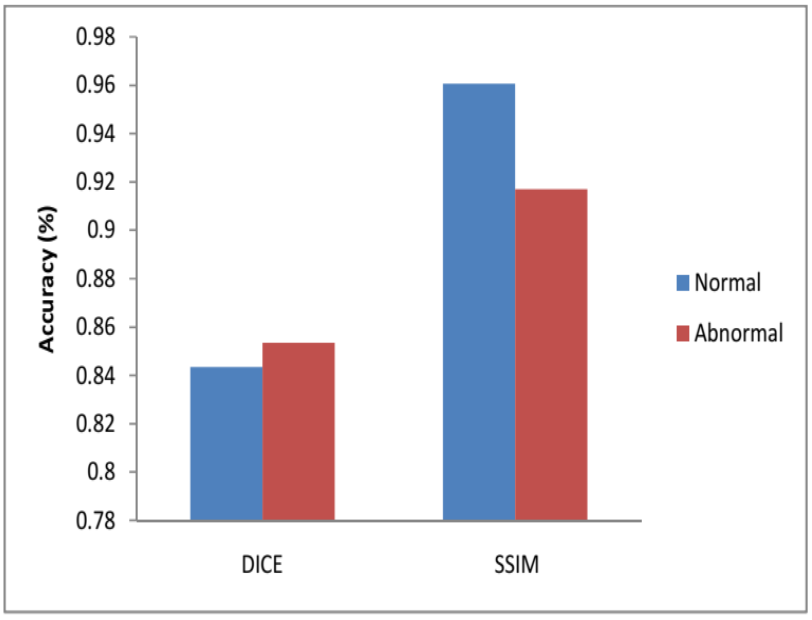

Figure 7: Segmentation Accuracy Performance

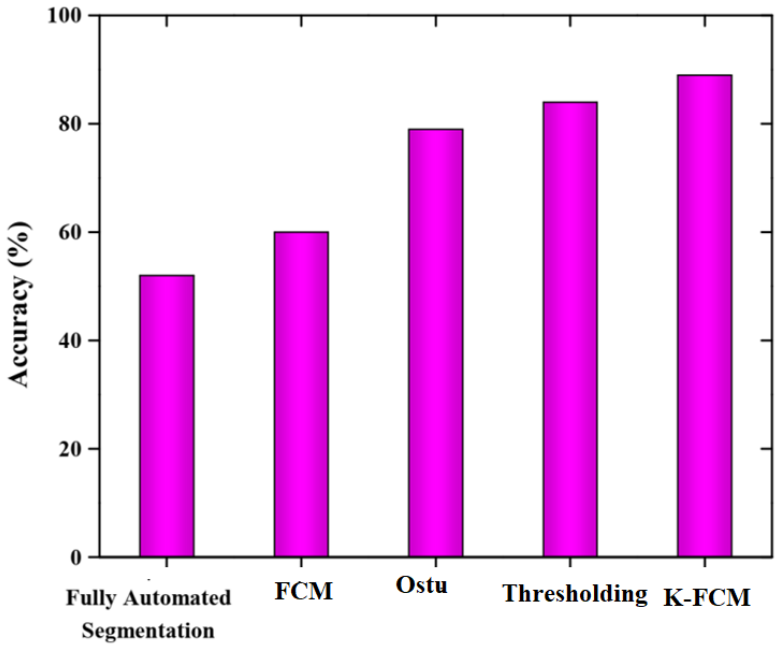

Figure 8: Segmentation Accuracy Analysis

Figure 8 presents the assessment of segmentation accuracy. The suggested K-segmentation FCM's accuracy is compared to that of existing segmentation approaches including fully automated segmentation, Thresholding, FCM, and Otsu. In small invariant cluster segmentation, threshold techniques like Otsu perform well, but not as well as other existing models and developed K-FCM algorithm. Clustering approaches such as FCM, Thresholding, and K-FCM have provided segmentation accuracy of 79 percent, 84 percent, and 89 percent, respectively. When compared to the above-stated model, the suggested K-FCM method achieved superior segmentation results.

Figure 9 shows a comparative study of the overall execution time graph. The entire execution time of the machine learning (ML) [10], machine learning and image processing (ML-IP) [12], dynamic graph cut method with a Naive Bayes (GC-NB) [13], deep learning (DL) [14] and suggested methods is determined. The total amount of time is calculated in seconds. According to the results, the suggested approach requires less time to execute than other algorithms such as ML, ML-IP, GC-NB, and DL.

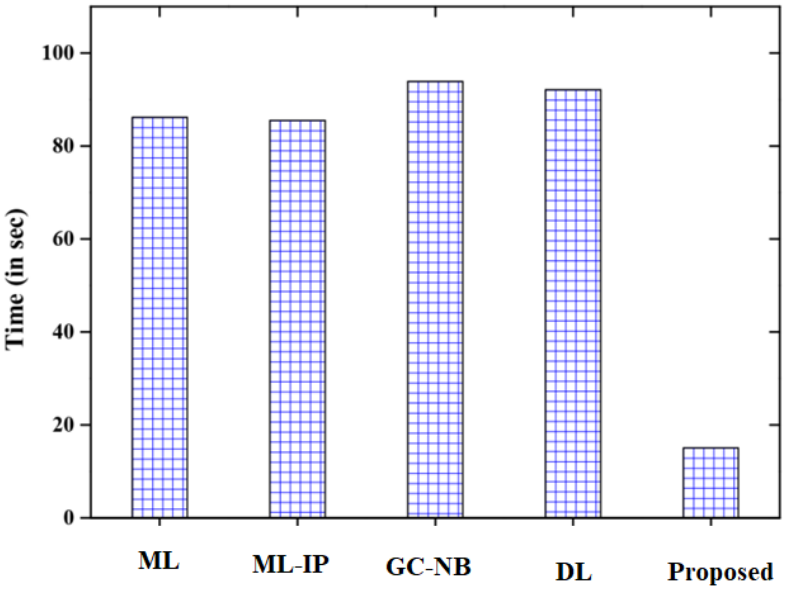

Figure 9: Segmentation Accuracy Results

Figure 10 presents the confusion matrix. The expected and actual categories of skin disease categorization accuracy based on normal and abnormal are described.

Actual Category		**Predicted Category**	
		Normal	*Abnormal*
	Normal	95%	5%
	Abnormal	8%	92%

Figure 10: Segmentation Accuracy Results

Figure 11 presents the comparative investigation of the overall detection performances. The performance of skin diseasedetection is validated using parameters like MCC, specificity, sensitivity, precision, and F-score with the ML, ML-IP, GC-NB, DL, and suggested technique. According to the findings, the proposed approach has an MCC of 99.27 percent, a specificity of 99.32 percent, a sensitivity of 99.02 percent, a precision of 99.34 percent, and an F-score of 99.27 percent. The developed model attained better outcomes than the conventional algorithms.

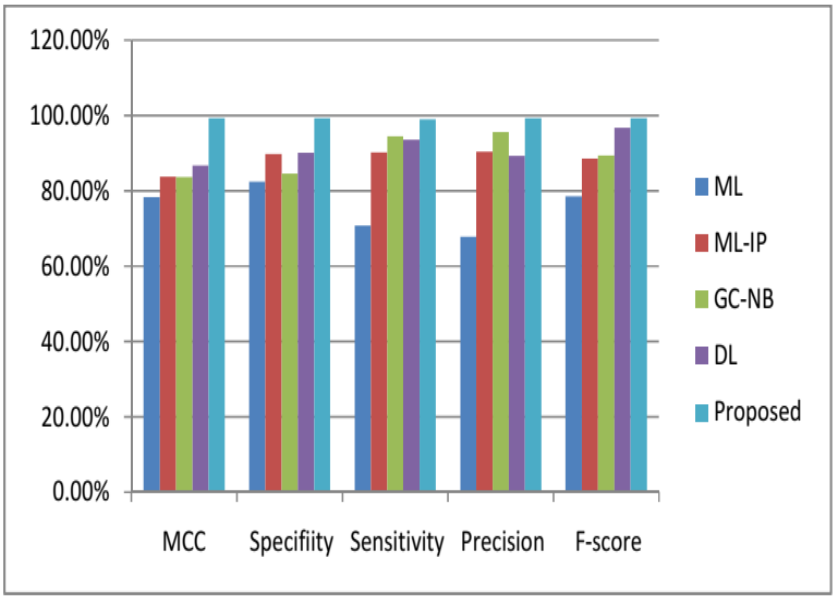

Figure 11:Overall Performance Kin Disease Classification

Conclusion

For skin disease categorization, this article presented a DLSTM-TSA for skin disease categorization. The database images were picked from the Herlev dataset in Denmark, and the MATLAB software was used as the execution framework. We used 70% of the entire number of images for training and 30% for testing out of the entire amount of photos. The original image is turned into various angles to evaluate the enhancement effectiveness. When employing K-FCM algorithms, a higher SSIM and DICE number suggests better segmentation outcomes.The suggested K-FCM approach outperformed the existing FCM, fully automated segmentation model, otsu, and Thresholding methods in terms of segmentation accuracy, with an 89 percent success rate. Using the suggested DLSTM-TSA superior prediction accuracy values are obtained, which are lower than those found using other current techniques such as ML, DL, GC-NB, and ML-IP.

Compliance with Ethical Standards

Conflict of interest

The authors declare that they have no conflict of interest.

Human and Animal Rights

This article does not contain any studies with human or animal subjects performed by any of the authors.

Informed Consent

Informed consent does not apply as this was a retrospective review with no identifying patient information.

Funding:

Not applicable

Conflicts of Interest Statement:

Not applicable

Consent to Participate:

Not applicable

Consent For Publication:

Not applicable

Availability of Data and Material:

Data sharing is not applicable to this article as no new data were created or analyzed in this study.

Code Availability:

Not applicable

References

[1] Kolkur, S. and Kalbande, D.R., 2016, November. Survey of texture based feature extraction for skin disease detection. In 2016 International Conference on ICT in Business Industry & Government (ICTBIG) (pp. 1-6). IEEE.

[2] Dubal, P., Bhatt, S., Joglekar, C. and Patil, S., 2017, November. Skin cancer detection and classification. In 2017 6th international conference on electrical engineering and informatics (ICEEI) (pp. 1-6). IEEE.

[3] Kolkur, S., Kalbande, D.R. and Kharkar, V., 2018. Machine learning approaches to multi-class human skin disease detection. International Journal of Computational Intelligence Research, 14(1), pp.1-12.

[4] Velasco, J., Pascion, C., Alberio, J.W., Apuang, J., Cruz, J.S., Gomez, M.A., Molina Jr, B., Tuala, L., Thio-ac, A. and Jorda Jr, R., 2019. A smartphone-based skin disease classification using mobilenetcnn. arXiv preprint arXiv:1911.07929.

[5] Okuboyejo, D.A., Olugbara, O.O. and Odunaike, S.A., 2013, October. Automating skin disease diagnosis using image classification. In proceedings of the world congress on engineering and computer science (Vol. 2, pp. 850-854).

[6] Ubale, A.V. and Paikrao, P.L., 2019. Detection and Classification of Skin Diseases using Different Color Phase Models. no. July, pp.1331-1335.

[7] Okuboyejo, D.A., Olugbara, O.O. and Odunaike, S.A., 2013, October. Automating skin disease diagnosis using image classification. In proceedings of the world congress on engineering and computer science (Vol. 2, pp. 850-854).

[8] Kumar, M. and Kumar, R., 2016. An Intelligent System to diagnosis the skin disease. ARPN JEAS, 11(19), pp.11368-11373.

[9] Ubale, A.V. and Paikrao, P.L., 2019. Detection and Classification of Skin Diseases using Different Color Phase Models. no. July, pp.1331-1335.

[10] Bhadula, S., Sharma, S., Juyal, P. and Kulshrestha, C., 2019. Machine learning algorithms based skin disease detection. International Journal of Innovative Technology and Exploring Engineering (IJITEE), 9(2).

[11] Chakraborty, S., Mali, K., Chatterjee, S., Anand, S., Basu, A., Banerjee, S., Das, M. and Bhattacharya, A., 2017, October. Image based skin disease detection using hybrid neural network coupled bag-of-features. In 2017 IEEE 8th Annual Ubiquitous Computing, Electronics and Mobile Communication Conference (UEMCON) (pp. 242-246). IEEE.

[12] ALEnezi, N.S.A., 2019. A method of skin disease detection using image processing and machine learning. Procedia Computer Science, 163, pp.85-92.
[13] Balaji, V.R., Suganthi, S.T., Rajadevi, R., Kumar, V.K., Balaji, B.S. and Pandiyan, S., 2020. Skin disease detection and segmentation using dynamic graph cut algorithm and classification through Naive Bayes classifier. Measurement, 163, p.107922.
[14] Khamparia, A., Singh, P.K., Rani, P., Samanta, D., Khanna, A. and Bhushan, B., 2021. An internet of health things-driven deep learning framework for detection and classification of skin cancer using transfer learning. Transactions on Emerging Telecommunications Technologies, 32(7), p.e3963.
[15] Yu, L., Chen, H., Dou, Q., Qin, J. and Heng, P.A., 2016. Automated melanoma recognition in dermoscopy images via very deep residual networks. IEEE transactions on medical imaging, 36(4), pp.994-1004.
[16] Chen, Y., Li, J., Zhang, H., Zheng, Y., Jeon, B. and Wu, Q.J., 2016. Non-local-based spatially constrained hierarchical fuzzy C-means method for brain magnetic resonance imaging segmentation. IET Image Processing, 10(11), pp.865-876.
[17] Memon, K.H. and Lee, D.H., 2018. Generalised kernel weighted fuzzy C-means clustering algorithm with local information. Fuzzy Sets and Systems, 340, pp.91-108.
[18] Wu, C. and Cao, Z., 2021. Noise distance driven fuzzy clustering based on adaptive weighted local information and entropy-like divergence kernel for robust image segmentation. Digital Signal Processing, 111, p.102963.
[19] Kolkur, S. and Kalbande, D.R., 2016, November. Survey of texture based feature extraction for skin disease detection. In 2016 International Conference on ICT in Business Industry & Government (ICTBIG) (pp. 1-6). IEEE.
[20] Chatterjee, S., Dey, D. and Munshi, S., 2019. Integration of morphological preprocessing and fractal based feature extraction with recursive feature elimination for skin lesion types classification. Computer methods and programs in biomedicine, 178, pp.201-218.
[21] Wang, F., Xuan, Z., Zhen, Z., Li, K., Wang, T. and Shi, M., 2020. A day-ahead PV power forecasting method based on LSTM-RNN model and time correlation modification under partial daily pattern prediction framework. Energy Conversion and Management, 212, p.112766.
[22] Messina, R. and Louradour, J., 2015, August. Segmentation-free handwritten Chinese text recognition with LSTM-RNN. In 2015 13th International conference on document analysis and recognition (icdar) (pp. 171-175). IEEE.
[23] Kaur, S., Awasthi, L.K., Sangal, A.L. and Dhiman, G., 2020. Tunicate Swarm Algorithm: A new bio-inspired based metaheuristic paradigm for global optimization. Engineering Applications of Artificial Intelligence, 90, p.103541.
[24] Houssein, E.H., Helmy, B.E.D., Elngar, A.A., Abdelminaam, D.S. and Shaban, H., 2021. An improved tunicate swarm algorithm for global optimization and image segmentation. IEEE Access, 9, pp.56066-56092.
[25] Yang, M., Tu, W., Wang, J., Xu, F. and Chen, X., 2017, February. Attention based LSTM for target dependent sentiment classification. In Proceedings of the AAAI Conference on Artificial Intelligence (Vol. 31, No. 1).
[26] Wu, D. and Chi, M., 2017. Long short-term memory with quadratic connections in recursive neural networks for representing compositional semantics. IEEE Access, 5, pp.16077-16083.
[27] Essaid, M., Kim, D., Maeng, S.H., Park, S. and Ju, H.T., 2019, September. A collaborative DDoS mitigation solution based on ethereum smart contract and RNN-LSTM. In 2019 20th Asia-Pacific Network Operations and Management Symposium (APNOMS) (pp. 1-6). IEEE.
[28] Agafonov, A.A. and Yumaganov, A.S., 2019. Bus arrival time prediction using recurrent neural network with LSTM architecture. Optical Memory and Neural Networks, 28(3), pp.222-230.
[29] Roy, S.K., Manna, S., Dubey, S.R. and Chaudhuri, B.B., 2019. LiSHT: Non-parametric linearly scaled hyperbolic tangent activation function for neural networks. arXiv preprint arXiv:1901.05894.
[30] Jerant, A.F., Johnson, J.T., Sheridan, C.D. and Caffrey, T.J., 2000. Early detection and treatment of skin cancer. American family physician, 62(2), pp.357-368.
[31] Jain, S. and Pise, N., 2015. Computer aided melanoma skin cancer detection using image processing. Procedia Computer Science, 48, pp.735-740.
[32] Sigurdsson, S., Philipsen, P.A., Hansen, L.K., Larsen, J., Gniadecka, M. and Wulf, H.C., 2004. Detection of skin cancer by classification of Raman spectra. IEEE transactions on biomedical engineering, 51(10), pp.1784-1793.
[33] Milton, M.A.A., 2019. Automated skin lesion classification using ensemble of deep neural networks in ISIC 2018: Skin lesion analysis towards melanoma detection challenge. arXiv preprint arXiv:1901.10802.
[34] Kinyanjui, N.M., Odonga, T., Cintas, C., Codella, N.C., Panda, R., Sattigeri, P. and Varshney, K.R., 2019. Estimating skin tone and effects on classification performance in dermatology datasets. arXiv preprint arXiv:1910.13268.
[35] Koh, H.K., Geller, A.C., Miller, D.R., Grossbart, T.A. and Lew, R.A., 1996. Prevention and early detection strategies for melanoma and skin cancer: current status. Archives of dermatology, 132(4), pp.436-443.
[36] Chaudhari, R., Vora, J.J., Mani Prabu, S.S., Palani, I.A., Patel, V.K., Parikh, D.M. and de Lacalle, L.N.L., 2019. Multi-response optimization of WEDM process parameters for machining of superelastic nitinol shape-memory alloy using a heat-transfer search algorithm. Materials, 12(8), p.1277.

[37] Chaudhari, R., Vora, J.J., Patel, V., López de Lacalle, L.N. and Parikh, D.M., 2020. Surface analysis of wire-electrical-discharge-machining-processed shape-memory alloys. Materials, 13(3), p.530.